Dou *et al.*
Chinese Journal of Mechanical Engineering (2023) 36:93
https://doi.org/10.1186/s10033-023-00918-1

Chinese Journal of Mechanical Engineering

ORIGINAL ARTICLE

Open Access

A Footpad Structure with Reusable Energy Absorption Capability for Deep Space Exploration Lander: Design and Analysis

Weiyuan Dou[1,2], Xiaohang Qiu[1], Zhiwei Xiong[3], Yanzhao Guo[1,2] and Lele Zhang[1,2*]

Abstract

The footpad structure of a deep space exploration lander is a critical system that makes the initial contact with the ground, and thereby plays a crucial role in determining the stability and energy absorption characteristics during the impact process. The conventional footpad is typically designed with an aluminum honeycomb structure that dissipates energy through plastic deformation. Nevertheless, its effectiveness in providing cushioning and energy absorption becomes significantly compromised when the structure is crushed, rendering it unusable for reusable landers in the future. This study presents a methodology for designing and evaluating structural energy absorption systems incorporating recoverable strain constraints of shape memory alloys (SMA). The topological configuration of the energy absorbing structure is derived using an equivalent static load method (ESL), and three lightweight footpad designs featuring honeycomb-like Ni-Ti shape memory alloys structures and having variable stiffness skins are proposed. To verify the accuracy of the numerical modelling, a honeycomb-like structure subjected to compression load is modeled and then compared with experimental results. Moreover, the influence of the configurations and thickness distribution of the proposed structures on their energy absorption performance is comprehensively evaluated using finite element simulations. The results demonstrate that the proposed design approach effectively regulates the strain threshold to maintain the SMA within the constraint of maximum recoverable strain, resulting in a structural energy absorption capacity of 362 J/kg with a crushing force efficiency greater than 63%.

Keywords Deep space exploration lander, Footpad, Shape memory alloy (SMA), Reusable energy absorption structure, Design method

1 Introduction

In order to realize multi-point detection (see Figure 1) and other scientific research activities on extraterrestrial bodies, reusable energy absorption structure gradually becomes one of the new requirements for soft landing of spacecraft [1–3]. In addition, the lander's energy absorption system should have the properties of being reusable, lightweight, and able to manage impact energy. Generally, the energy absorbed structure of the soft-landing system, such as the landing leg and footpad, dissipates the energy induced by impact during the landing process. The energy absorbing behaviors of the footpad, as the primary cushioning unit that contacts the target first, have a direct influence on the landing leg's energy absorption modules, as well as the overall payload system's dynamic response [4, 5].

At present, there are numerous types of energy absorption structures, and the energy dissipation mechanisms

*Correspondence:
Lele Zhang
llzhang1@bjtu.edu.cn
[1] School of Mechanical, Electronic and Control Engineering, Beijing Jiaotong University, Beijing 100044, China
[2] National International Science and Technology Cooperation Base on Railway Vehicle Operation Engineering, Beijing Jiaotong University, Beijing 100044, China
[3] China Academy of Space Technology, Beijing 100094, China

for these structures are diverse. Aluminum honeycomb, the most representative and widely used energy absorption structure, has excellent energy dissipation performance due to its high strength-to-weight ratio [6–9]. Remarkably, it has been successfully used in the United States' Apollo 11, which is also known as the first crewed mission to land on the moon. As well as the Chinese lunar exploration program, such energy absorption structures are used in the landing gear system of Chang'e. By employing aluminum honeycomb, the landing gear is simple, has great adaptability and reliability, and can satisfy the demands of supplying various payload systems through a sensible design [10–12]. However, the aluminum honeycomb can be used only once due to its energy dissipation mechanism, i.e., the plastic dissipation of metallic material. In terms of reusable energy absorption structures, metal rubber, hydraulic, mechanical, and electrical/magnetic rheological are the most common types [13–15]. At this point, energy absorption structures of the aforementioned types can serve as reusable landing gears. Unfortunately, they have to face the problems such as complexity, reliability, and energy dissipation performance (significantly lower than one-time used landing gears at equal mass).

Shape memory alloy (SMA) is a so-called smart material with the characteristics of superelasticity, shape memory effect (SME) and high damping [16, 17]. Benefited from these properties, SMA has a potential to be used in the future to design a reusable landing gear. NiTi-based material is one of the most commonly used SMA material, and its superelastic strain can usually exceeds 8% [18, 19]. In addition, the maximum superelastic strain of Cu-based SMA (such as Cu-Al-Be) can reach 23% [20, 21], and 13% for Fe-based SMA [22]. The stress-strain curve of superelastic SMAs show a flag like hysteresis loop under cyclic load. Such hysteresis characteristic has the advantages of energy dissipation and minimum residual deformations upon load release. NASA developed a SMA wire fabricated wheel with this property so that it can run smoothly over the complex surface of extraterrestrial planets [23]. On the other hand, a SME-based energy absorption structure can be deformed when cold but returns to its original shape when heated, allowing the structure to be reused multiple times within a certain range of strain. In Ref. [24], the recoverable strain could exceed 5%. SMA-based structures are typically made by casting, using vacuum arc melting or induction melting [25]. The challenges of processing SMA-based structure with complex configuration can be overcome by additive manufacturing technology. NiTi-based SMA fabricated by Selective laser melting (SLM) has an elongation as high as 15.6% [26]. By heating up after 50% compression deformation, honeycomb-like structures and lattice structures made of SMA materials can achieve a shape recovery rate of more than 98% [27, 28], which provides a new idea for the design of reusable energy absorption structure. In general, SMA materials have the ability of regaining their original shape after being deformed. As they can absorb energy through deformation and then return to their original shape, they are ideally suited for reuse in energy-absorbing structures.

In order to develop effective energy absorption structures while taking lightweight constraints into consideration, numerous numerical simulations and experimental research have been methodically carried out on the design of macroscopic structure and multi-cell structure. In order to address the nonlinear problems (such as plastic hinges, nonlinear material properties, and others) in the topology optimization of the structures under dynamic loads, specific solutions are required for the macro-configuration optimization of crashworthiness structures. Kang et al. [29] proposed an equivalent

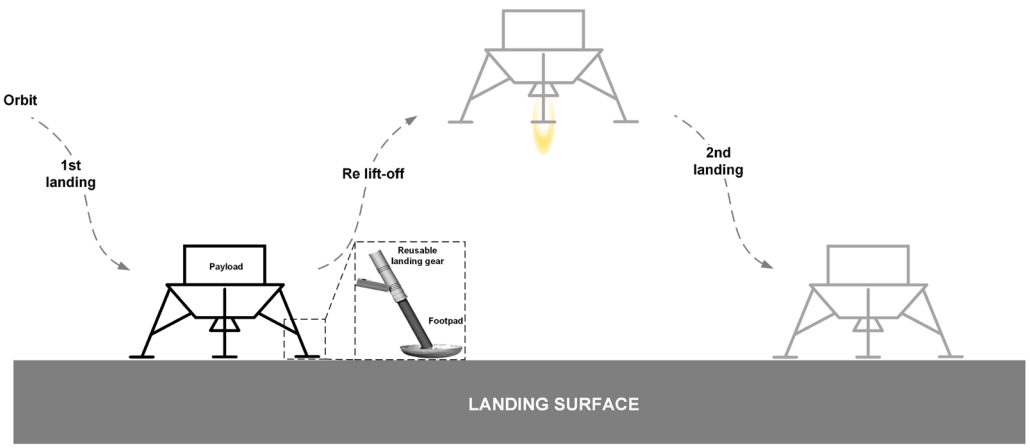

Figure 1 A conceptual design for multi-point detection of a lander

static loads method (ESL) and applied it to optimize the size and shape of linear dynamic systems. Subsequently, Park et al. [30] proved that the ESL-based optimization approach satisfies the Karush-Kuhn-Tucker condition and is mathematically identical to the direct dynamic optimization method. With the improvement of computational efficiency, the ESL method was utilized to optimize the topology of the front-end crashworthiness structure of automobiles [31], resulting in a significant weight reduction and improvement on its crash performance. Based on this approach, Patel et al. [32] extended the Hybrid Cellular Automata method (HCA) to crashworthiness topology optimization; Aulig et al. [33] used this method to optimize a white car-body structure under the comprehensive conditions of structural collision and static loading, and a balanced result was obtained through multi-condition optimization.

On the other hand, considering that large rotation and large strain deformation modes of structures (e.g., plastic hinge) are usually unavoidable in the collision, the introduction of multicellular structures allows for adequate energy dissipation of materials as well as the guidance and control of structural deformation. Nia et al. [34] designed and analyzed the specific energy absorption of triangle, square, and other multi-cell polygonal tubes under axial compression load, and found that thin-walled tubes with multi-cell structures show better performance in terms of energy absorption. He et al. [35] presented a thin-walled energy absorption tube with hierarchical properties based on Sierpinski fractal structure, and family structures from the first to the third order are introduced in this study. The findings indicate that the implementation of Sierpinski hierarchy significantly increases energy absorption capacity, and the mean crushing force of the three tubes tends to rise by 70.5%, 113.2%, and 150.1%, as compared to the single-cell triangular (ST) tubes under the same relative density. Abdullahi et al. [36] proposed a novel square-section tube filled with Voronoi cells, and the results demonstrated that the initial peak force of the designed tube is lower than that of a multicellular square tube of the same size, but the specific energy absorption of the proposed tube is greater. A tube-like energy absorption structure with Voronoi configuration on the side wall was proposed to study its performance under in-plane compression load, and the results revealed a negative correlation between the cell's inhomogeneity and the structure's energy absorption capacity [37]. By introducing small triangular structure in each vertex of a regular hexagonal honeycomb, the plateau force and specific energy absorption increased by 127% and 109% along the in-plane direction [38]. As can be seen, compared to conventional square tube, round tube, and other regular cross-section structures, multi-cell energy absorption structures could give superior energy dissipation performance, particularly for higher specific energy absorption and lower initial peak force.

In conclusion, a SMA-based multi-cell structure fabricated through additive manufacturing technology shows decent potential in the areas of reusable energy absorption structures. However, if the structural deformation exceeds the maximum recoverable strain of the SMA material, the repeatable energy absorption threshold of the entire structure will be diminished or partially lost. Therefore, the constraint of maximum recoverable strain of SMA should be taken into account in the design, and the energy dissipation capacity of materials should be thoroughly investigated through an integrated design of the macroscopic configuration (e.g., structural topology optimization) and the secondary configuration (e.g., multi-cell structure).

In this study, we focus on the design method of a reusable footpad structure for deep space exploration landers. A design method for the energy absorption structure that considers the recoverable strain of shape memory alloys as a design constraint is proposed, aiming to achieve the reusability of the structure after cushion deformation through the memory effect of shape memory alloys. Specifically, crashworthiness topology optimization method is employed to determine the macroscopic configuration of the entire footpad structure. Numerical simulations are performed to investigate the energy absorption characteristics of the designed NiTi-based SMA footpad. In terms of secondary configuration, the influence of local cell design variables on structural deformation modes and energy absorption performance is thoroughly investigated in this work. By doing so, it can provide preliminary investigations and basis for a comprehensive design of the energy absorption structure of a reusable lander in the near future.

2 Fundamentals

Over the past few decades, significant developments have been made in constitutive models for shape memory alloys. Uniaxial, largely empirical relations have developed into more and more sophisticated mathematical representations of the effects seen in these materials [39]. According to the methods used in describing the behavior of shape memory alloys, they can be categorized as microscopic thermodynamic model, micro-macro model, macroscopic model, and etc. For example, the Helmholtz free energy density of the constitutive model is postulated to be of the form

$$W(\varepsilon, \varepsilon_m, \lambda, T) = \frac{1}{2}\varepsilon_e : \sigma + \lambda L \frac{T - T_C}{T_C} - c(\lambda) T \ln\left(\frac{T}{T_C}\right) + \lambda G_i(\varepsilon_m) + G_s(\lambda \varepsilon_m) + G_\lambda(\lambda), \tag{1}$$

where ε, ε_e, ε_m are the total strain, elastic strain, and martensite strain, respectively; $\lambda \in [0, 1]$ is the volume fraction of martensite. The first three terms in W are strain energy density, chemical energy density of martensite, and the thermal energy density; and the last three terms describe energy densities for martensite initiation, saturation and transformation. Accordingly, the afore-mentioned thermodynamics-based model, while providing a more reasonable depiction of shape memory effects, encounters significant challenges due to the involvement of so many unknown variables. Consequently, solving the finite element equations demands substantial computational resources, with convergence issues posing a major obstacle as well. In this case, the applicability of such constitutive model for solving large-scale complex models is currently limited, and its direct utilization in the design of energy absorption structures based on shape memory alloys is still impractical.

It is noteworthy that the stress-strain curve of the SMA material with shape memory effect shows a piecewise linear behavior before the maximum recovery strain (see Figure 2). Regardless of the thermodynamics when it is heated until recover to its original shape, the mechanical property is somehow similar to an isotropic plastic material. That is to say, when we are focusing on the performance of the SMA material or structures in a certain condition, i.e., loading process, a piecewise linear plasticity material model can be implemented in the FE analysis. The plastic response of the material is segmented into a series of linear segments. For example, MAT_024 in LS-DYNA, this model is widely employed within the fields of computational mechanics and engineering to analyze the deformation and failure of materials subjected to substantial strains.

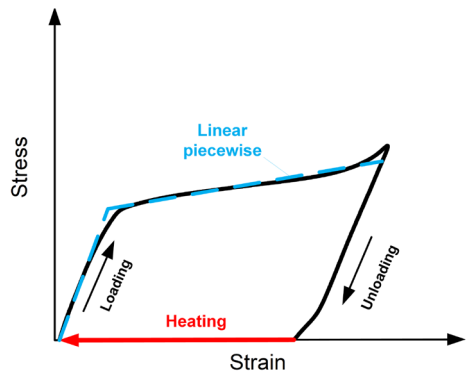

Figure 2 The shape memory effect process of a typical SMA, and a linear piecewise characterization

To design a SMA-based reusable footpad of a lander, the mechanical performance of the structure and the recoverability of the material under large deformation should be taken into account. As shown in Figure 3, to address the aforementioned issues, three steps are involved in this study.

Step 1: In order to optimize the geometry of the energy absorption structure, a topology optimization method based on the ESL method is initially implemented. The optimization algorithms consider the trade-off between weight reduction and crash performance, and iteratively modify the geometry and topology of the structure until the optimal solution is found. The original configuration of the energy absorption structure in the footpad is fixed in the initial stage design while taking into consideration the practical boundary conditions.

Step 2: The energy absorption structure of the footpad is then replaced by honeycomb-like cellular structures based on the original shape. The various configurations are introduced and compared through finite element analysis. To validate the accuracy of the modeling methodology and numerical simulation, a representative SMA honeycomb-like structure fabricated via additive manufacturing is also investigated.

Step 3: In this study, the energy absorption performance of the redesigned footpad is thoroughly evaluated by considering the maximum recoverable strain of the SMA alloy as a constraint. The mechanical properties of the footpad under impact loading are analyzed by varying the wall thickness of different components.

To evaluate the energy absorption capacity, several criteria have been employed. Energy absorption (EA) of structures under impact load can be expressed as:

$$\mathrm{EA} = \int_0^\delta F(s)\mathrm{d}s, \tag{2}$$

where δ and F represent the compression distance and corresponding load.

The peak crushing force (PCF) refers to the maximum force applied to a structure during a crushing process:

$$\mathrm{PCF} = \max(F(s)). \tag{3}$$

The mean crash force (MCF) is typically calculated as the total force applied over a certain period of time divided by the duration of the crushing process:

$$\mathrm{MCF} = \frac{\mathrm{EA}}{\delta}. \tag{4}$$

Crushing force efficiency (CFE) represents the proportion of applied force that is actually utilized to crush the

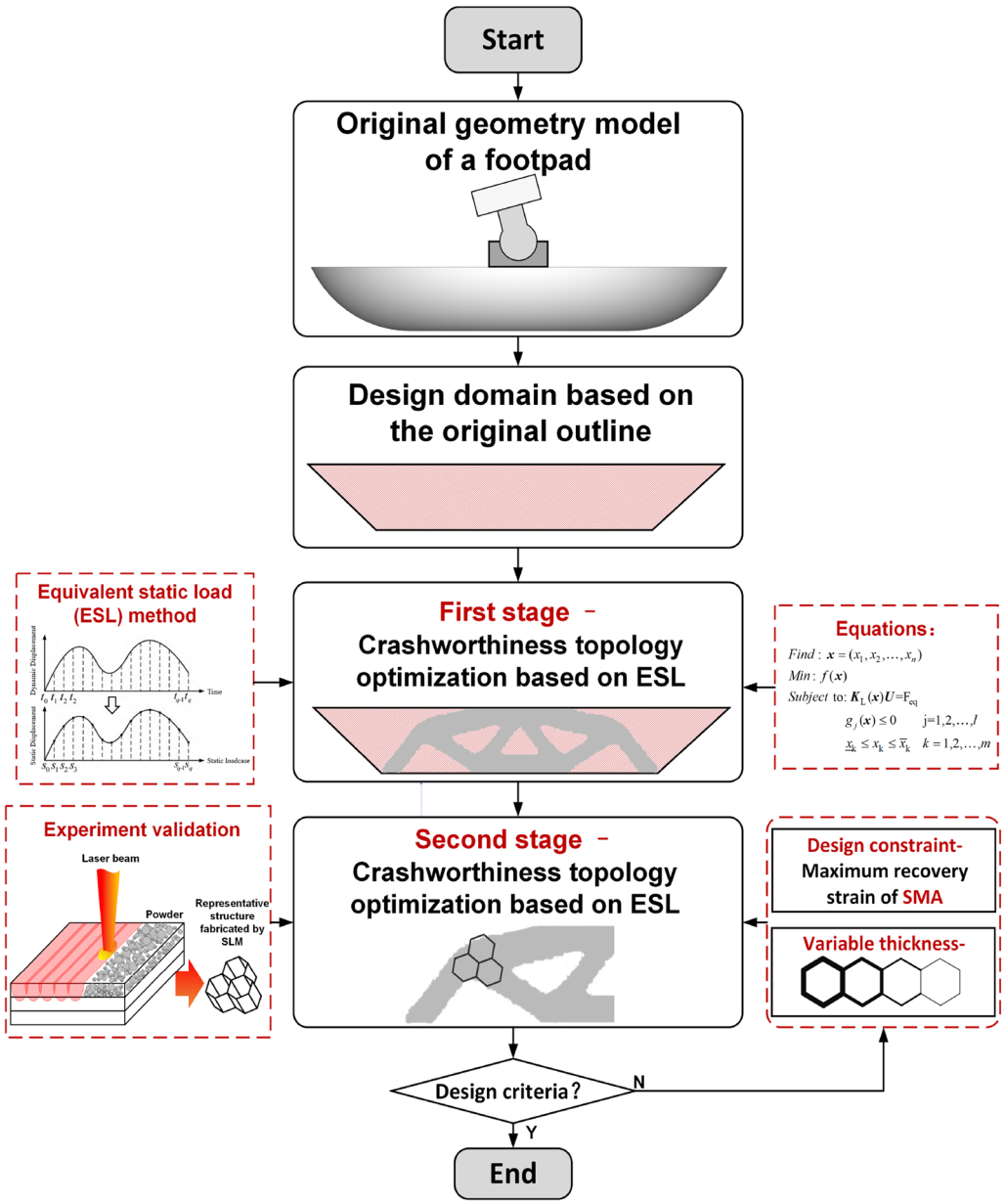

Figure 3 A flowchart illustrating the footpad design process

material. By improving the CFE of a crushing process, it is possible to reduce the amount of energy required to produce a given quantity of crushed material, leading to cost savings and increased sustainability:

$$\mathrm{CFE} = \frac{\mathrm{MCF}}{\mathrm{PCF}}. \tag{5}$$

Specific energy absorption (SEA) is determined by measuring the amount of energy that the material absorbs upon impact. Energy absorption structures with higher SEA values are capable of absorbing more energy per unit of mass, and are therefore considered to be more effective in reducing impact energy:

$$\mathrm{SEA} = \frac{\mathrm{EA}}{m}, \tag{6}$$

where m is the total mass of the energy absorption structure.

3 Design of a Footpad and Numerical Modeling

3.1 ESL-based Structural Topology Optimization

The equivalent static load (ESL) method [40] is described as follows: the response induced by the structure's static load in the linear static analysis is identical to the response generated by the dynamic nonlinear analysis at the same time step. In other words, the time domain $[0, t]$ is discretized into q time steps in the optimization of dynamic problems based on the ESL approach in order to obtain equivalent static loads and corresponding conditions based on equivalent static response analysis, as shown in Figure 4.

ESL-based optimization has been widely used in nonlinear analysis and structural design problems. ESL-Dyna is an optimization implementation of the ESL method based on LS-DYNA solver, while GENESIS is an optimization software for linear problems. Figure 5 shows the process of ESL-based topology optimization.

Step 1: Read the ESL related parameter files, and create new input files for GENESIS optimization and LS-DYNA.

Step 2: Set the initial material factor for each element in the FE model to 0.3, in order to presume that the material seed can provide a feasible solution to the optimization issue.

Step 3: Set initial value: iteration number $k = 0$, initial value of design variable $\boldsymbol{x}^{(0)} = (x_1, x_2, ..., x_n)$, and set it to 1% according to the common engineering error. At the same time, the maximum cycle $k_{\max}$ of topology optimization iterations is defined.

Step 4: Complete the dynamic nonlinear calculation and analysis of the model by utilizing LS-DYNA.

Step 5: The nodal displacements obtained from LS-DYNA calculations are introduced, and the time-course curves are divided into $n-1$ subintervals. The linear stiffness matrix $\boldsymbol{K_L}$ of the structure of n time nodes was successively calculated and multiplied with the displacement vector of the nodes $\boldsymbol{U}$ to obtain the equivalent static load $\boldsymbol{f_{eq}}$:

$$\boldsymbol{f_{eq}} = \boldsymbol{K_L}(\boldsymbol{x})\boldsymbol{U}(\boldsymbol{t_e}). \tag{7}$$

Step 6: The equivalent static load is reapplied to the structure, and linear static analysis is conducted to optimize the structural topology. Check the convergence criteria.

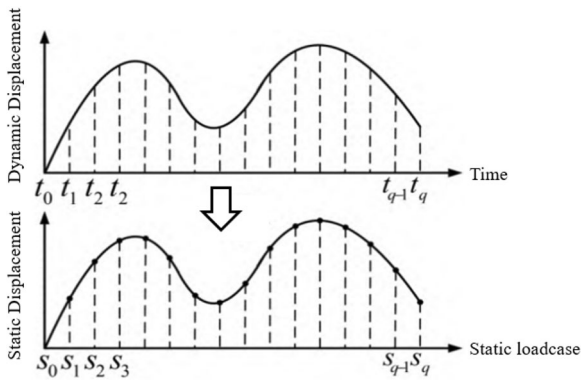

Figure 4 Definition of the equivalent static load method

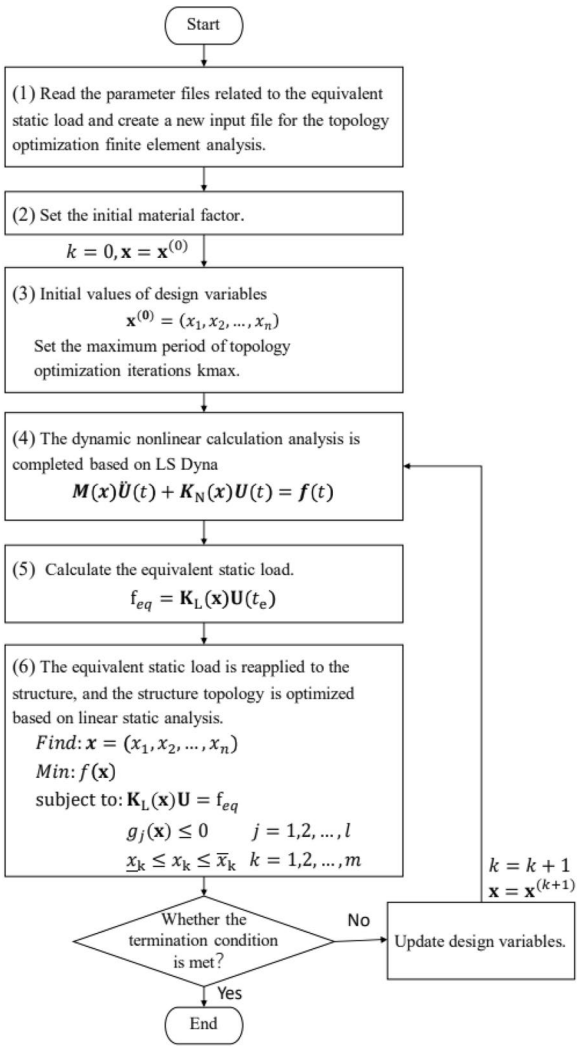

Figure 5 Flowchart of the topology optimization procedure using ESL-Dyna

3.2 Topology Optimization of a Footpad Subjected to Impact Load

The appearance of the lander's footpad is a bowl like solid of revolution. Considering the geometry configuration of the lander's footpad, the design domain is denoted by a cross section. As shown in Figure 6a, the fillet of the cross section is diminished, and then the design domain of the

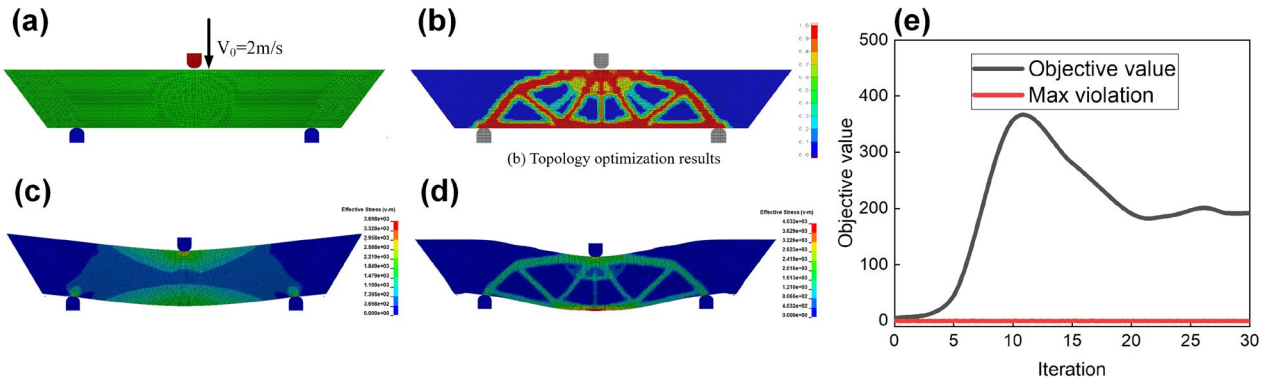

Figure 6 Topology optimization of a footpad subjected to impact loading: **a** Design domain obtained from the original geometry model, and boundary conditions in numerical simulations, **b** Topology optimization results configuration, **c** Stress contour of the design domain prior to optimization, **d** Stress contour of the topology optimization results, **e** Convergence curves for the objective value and maximum violation during the optimization process

section is represented by an inverted trapezoid configuration. In the terms of the cross section, 2D plane stress element is employed to implement topology optimization process. The entire structure was discretized using plane stress elements with a thickness of 0.5 mm and a size of 2 mm. The discretized model has a total of 10600 elements and 10886 nodes, respectively.

When a lander is on its mission during a soft landing process, the surface irregularity of the target may have a significant influence on the landing dynamic performance [41, 42]. In particular, the first points of contact usually occur between small rocks and the footpad's bottom surface, for which non-uniform compression is suspected throughout the landing process. Three-point bending deformation [43] is one of the footpad's critical conditions, and its topological configuration is more complex than that of a simple compression condition. Therefore, a three-point bending based topology optimization on the footpad is conducted in this study.

Regarding the boundary conditions of the numerical simulation model, two supporting pins a set distance apart are employed to simulate the rocks, and a single loading indenter at the middle is used to transfer the load to the footpad (see Figure 6a). Specifically, the rigid supports are fixed, and the indenter is set to move at a speed of 2 m/s. Both the supporters and the indenter are modeled using a rigid material model MAT20, while the footpad is modeled using the elastoplastic material model MAT24 in LS-DYNA. In addition, 2D-automatic contact was utilized in the contact patches, namely between the upper surface of the footpad and the indenter, and the lower surface of the footpad and the supports.

It should be noted that ESL is a topology optimization approach for designing structures subjected to static loads. Creating an equivalent static load case that simulates the effect of the applied loads and then employing it in a typical static analysis are the steps involved. The resulting stresses, deformations, and strains are then utilized as design variables to construct an optimized structure. In practical applications, the topological configuration is widely used as a reference model, sometimes known as a prototype. In this case, steel material properties with Young's modulus $E = 200$ GPa, Poisson's ratio $\nu = 0.3$, yield stress $\sigma_y = 300$ MPa and plastic hardening modulus $E_p = 0.3E$ are used in the optimization. On the other hand, the optimization objective is to minimize the strain energy of the structure, while ensuring that the mass fraction of the footpad structure is maintained at 0.35. It is required that the maximum displacement of the indenter not exceed 20 mm, and the allowable maximum crushing force is set to be 20 kN. As shown in Figure 6e the optimization calculation converged after 30 iterations, and the maximum violation value almost keep zero during this process. The final obtained design configuration, effective stress contours for the footpad before and after topology optimization are shown in Figure 6b–d, respectively. After removing 65% of the material, it can be observed that the optimal design is an inverted trapezoidal configuration under impact load. In this case, the outer-ring material of the footpad's design domain contributes less to energy absorption.

3.3 Redesign of the Footpad with Honeycomb-like Configuration

Several studies have demonstrated that honeycomb-like and multiple segment structures with varying stiffness can perform sequential structural deformation, reduce the initial peak of crushing force, and make the load curve much more stable under in-plane compression conditions [44]. Lightweight cellular structures that

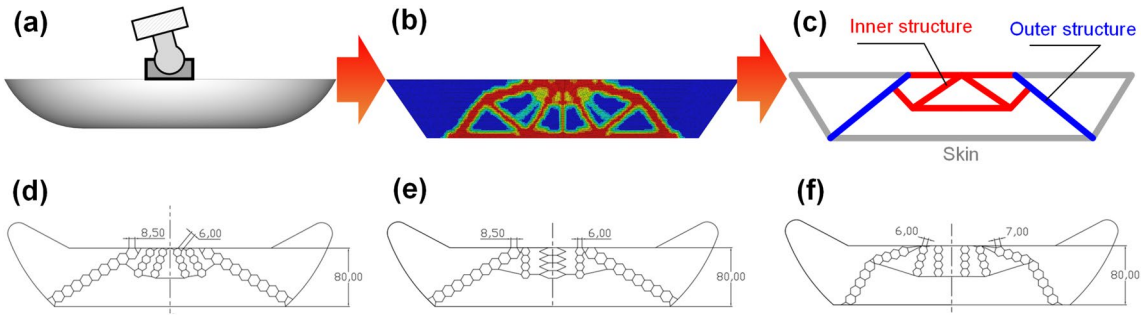

Figure 7 Three footpad models with different configurations based on topology optimization results: **a** Original geometry model in application, **b** Configuration obtained from topology optimization, **c** Conceptual design incorporating inner structure, outer structure, and skin, **d** Model-I, **e** Model-II, **f** Model-III

provide a high energy absorption capacity due to their large deformation and energy dissipation through bending and shearing. On the footpad, the load transferred from the landing leg acts in a vertical direction, as shown in Figure 7a. It is noticeable from the topology configuration of the footpad that the compression load is shared by the inner and outer structures. Both these two components will deform simultaneously upon impact load.

As a prototype, the inner structure and outer structure obtained from the derived topology optimization results are then maintained. By introducing the design concept of two-stage energy absorption modules, the height of the inner structure is reduced to achieve variable footpad stiffness. That is, the outer structure deforms first when the bottom of the footpad hits the target, which can also contribute lateral stiffness to restricting unbalanced load along this direction. With increasing deformation of the outer structure, the bottom of the inner structure tends to contact the bottom of the footpad and behaves as the secondary stage of the energy absorption structure. In this case, the initial peak crashing force may be properly controlled, and the energy-absorption structure will deform sequentially from the outer to the inner structure. This form of structure is introduced as Model I in this study.

Generally, honeycomb-like structures exhibit two distinct forms of deformation: compression and shear deformation [45]. The shear deformation usually occurs when the configuration of the cells is discordant with the loading direction. This mode will also result in low energy absorption efficiency and structural stiffness due to the shear deformation of the cells. In order to avoid shear deformation of cells, the oblique inner structures of Model I are modified to a vertical distribution, and the resulting structure is defined as Model II. In addition, based on Models I and II, the outer structures are divided into two segments with different angles to reduce shear deformation of straight structures under compression

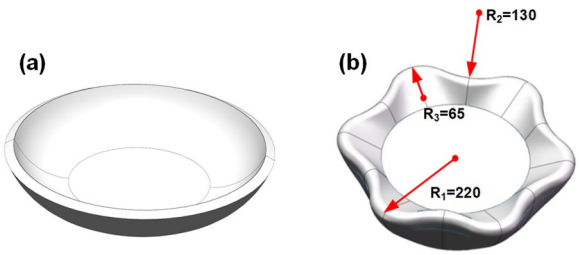

Figure 8 Comparison of two footpad geometry models: **a** Traditional bowl-shaped circular footpad, **b** Redesigned footpad with curvature configuration

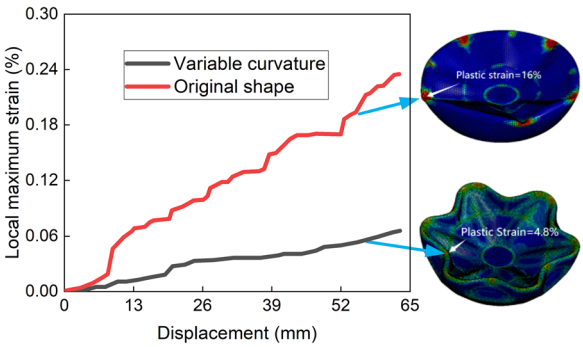

Figure 9 The maximum strain curves for the footpads subjected to compression load

loads. And then, the model with this configuration is defined as Model III, as shown in Figure 7d–f.

According to the operating conditions of the foot pad of the lander, the skin of the foot pad serves to protect the interior structure and prevent dust. During the landing process, the outer skin of the footpad will deform simultaneously with the inner energy absorption structures. In general, the footpad of the lander is a bowl-shaped structure with a circular configuration; when the footpad is impacted under impact load, several plastic hinges may be observed locally, as shown in Figure 9.

Specifically, local strain values over 10% at these plastic hinges will have a considerable effect on the reusability of the footpad. As explained previously, too large strain has a detrimental impact on the recoverability of NiTi shape memory alloy based structures.

Therefore, the outer skin of the footpad will be redesigned to prevent excessive strain caused by the local plastic hinge. In this study, a novel footpad configuration with variable curvature (see Figure 8) is proposed to stabilize the footpad's deformation under compression load. In Figure 9, it can be seen that the deformation of the footpad with curvature configuration is much more uniform than the original design. The maximum strain of the footpad with curvature configuration is 30% lower than that of the circular footpad at the same compression distance. When the compression distance is 60 mm, the maximum strain in the circular footpad is approximately 23%, which is greater than the material's tensile strength. However, the maximum strain in the curvature configuration footpad is less than 5%, which significantly reduces the high strain induced by the local plastic hinge.

3.4 Numerical Modeling and Validation

Considering the constraints imposed by the maximum manufacturing dimensions, a representative structure is selected for the purpose of evaluating its mechanical properties under a specific loading condition. Additionally, this structure also serves as a means of validating the accuracy of the numerical modeling method employed in this study. Figure 10 shows the stress-strain curve of a SLM fabricated NiTi alloy tensile sample, in which the inset is the tooling and the measurement extensometer. Prior to deformation testing, the specimen is cooled below 0 °C to ensure the martensitic state. The basic mechanical properties of NiTi are as follows: Young's modulus $E=18$ GPa, Poisson's ratio $\nu=0.3$, yield stress $\sigma_y=132$ MPa, density $\rho=6450$ kg/m^3.

Using the same processing parameters, a 5×4 cells NiTi honeycomb structure is fabricated in order to examine its mechanical performance under compression load. As shown in Figure 11, the size of the honeycomb structure is 80 mm × 90 mm × 10 mm. The length of each side and thickness of a single cell are 11 mm and 0.4 mm, respectively. And then, a in-plane compression is conducted by utilizing a universal testing machine.

Regarding finite element modeling of the honeycomb structure, the geometry model is discretized using the Belytschko-Tsay shell element with an element size of 0.5 mm. The numerical simulation involves a total of 36145 elements and 37322 nodes, respectively. The interactions between the honeycomb structure and the rigid plates are defined as automatic single-surface contacts, whereas automatic surface-to-surface contacts are utilized for the contacts between the cell side walls. The lower rigid plate is fixed and the upper rigid plate is subjected to a constant velocity of 0.3 m/s. The friction coefficient used in the contact algorithm is set as 0.17.

Figure 12a shows the deformation of the honeycomb structure under different compression distance. During the whole process, no shearing band is observed among the cells, and the deformation of the structure is stable and sequential as expected. Specifically, the core cells of the honeycomb yields to the pressure load first, and then the other cells surrounded the cores deforms in order. In terms of the numerical simulation, it can be seen that the structural deformation at different compression rate is well consistent with the experimental results (see Figure 12b). Two monitoring points are fixed in the side wall of one core cell, and the total strain of the certain points in simulation and experiment are then compared jointly. Figure 12c, d demonstrate the strain curves of the monitoring points and the pressure load curves subject to the honeycomb structure. Comparing simulation with

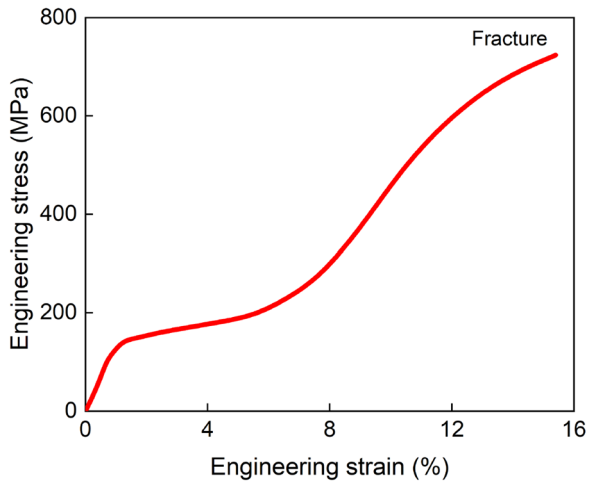

Figure 10 Tensile stress–strain curve of the SLM fabricated NiTi specimen

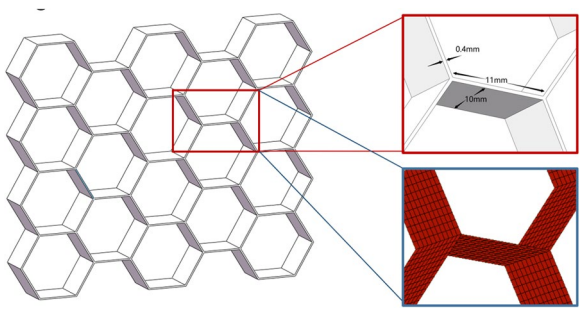

Figure 11 Geometric model of a honeycomb-like structure and mesh discretization for finite element analysis

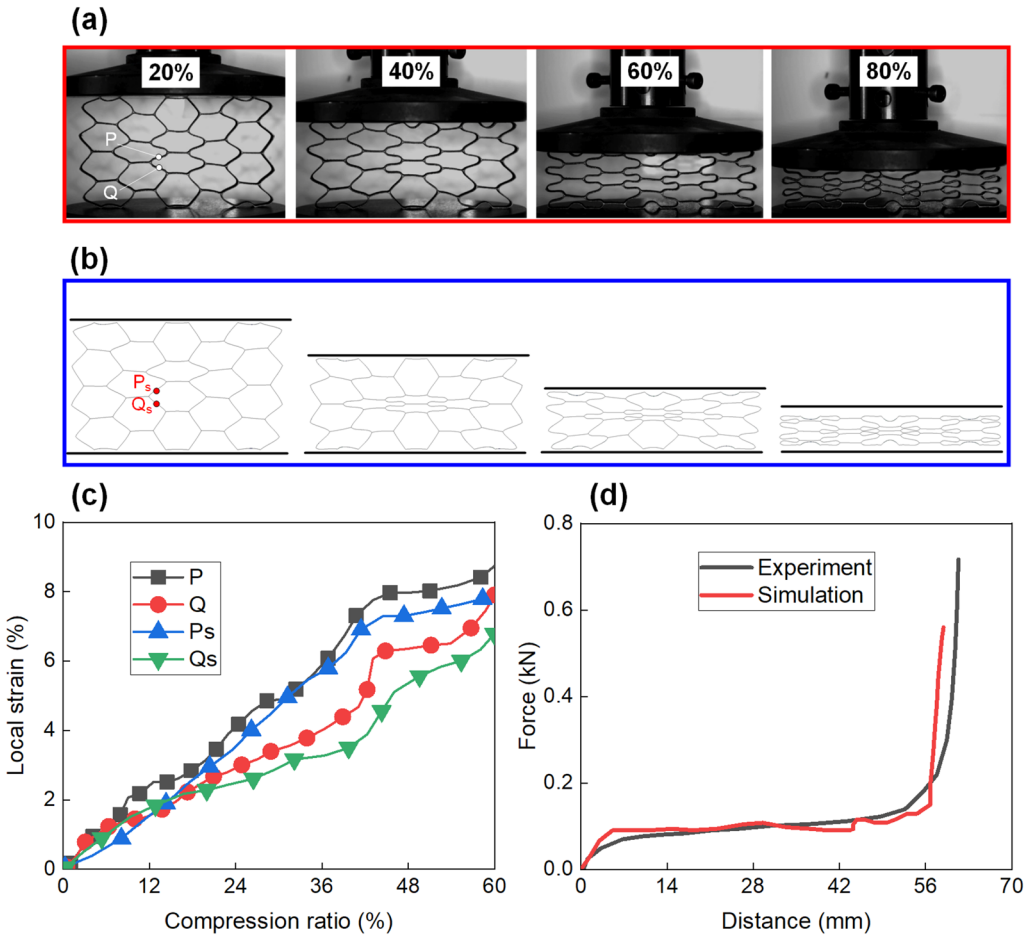

Figure 12 Comparison of experimental and simulation results for the compression of a honeycomb-like structure: **a** Deformation results at compression rates of 20%, 40%, 60%, 80% from experiments [28], **b** Deformation results of a shell element-based finite element model subjected to compression load at the same compression rate in experiment, **c** Comparison of local strains at two monitoring points in experiment and simulation, **d** Force-compression distance curves for experiment and simulation

experiment results, the mean square error of the two monitoring points is 1.0×10^{-4} and 1.1×10^{-4}, respectively. And the mean square error between two global pressure load curves is 1.5×10^{-4}. In conclusion, the modelling method for the honeycomb-like structure fabricated by NiTi alloy can provide a reasonable result for numerical simulations. With the same set up, more complex structural configuration design will be further investigated in the following sections.

4 Results and Discussion

4.1 Comparison of Different Configurations Based on the Topology Results

In this section, three distinct configurations of the designed footpad structure are presented for the investigation of their energy dissipation characteristics under impact loads. The wall thickness of both the inner and outer structures is set as 0.71 mm, and the total mass of the footpad is 2.5 kg.

As shown in Figure 13, in the compression process of configurations 1 and 2, the outer energy absorption structure undergoes initial deformation followed by cell shear deformation. However, no appreciable shearing behavior is observed in Model-III. Upon reaching a compression displacement of approximately 30 mm, the lower portion of the inner structure comes into contact with the ground, leading to gradual crushing of the cells in this region.

Due to the limitation of the maximum recoverable strain $\varepsilon_{\max}^{rec}$, the more uniform the strain distribution in the structure, the greater the amount of energy that may be absorbed before the value of $\varepsilon_{\max}^{rec}$ is reached. When the overall compression is 60%, the differences between the maximum strains and the minimum strains of three configurations' inner honeycomb structures are

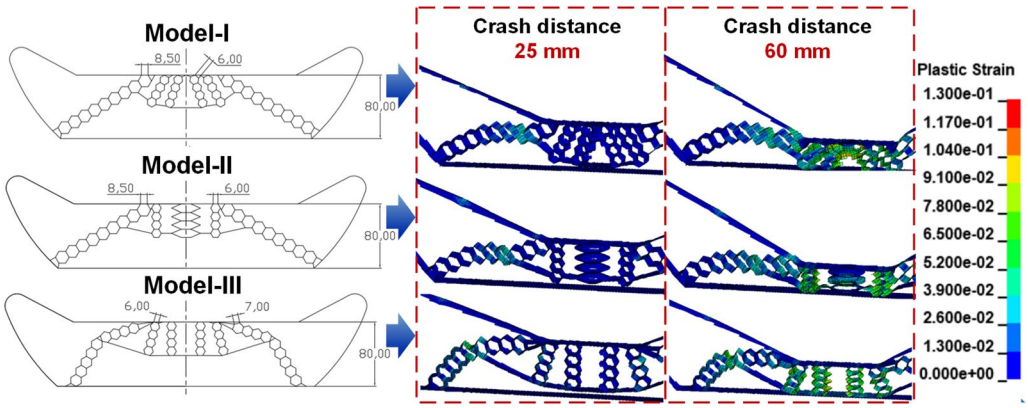

Figure 13 Strain contours and deformation results for three models with varied configurations based on simulation

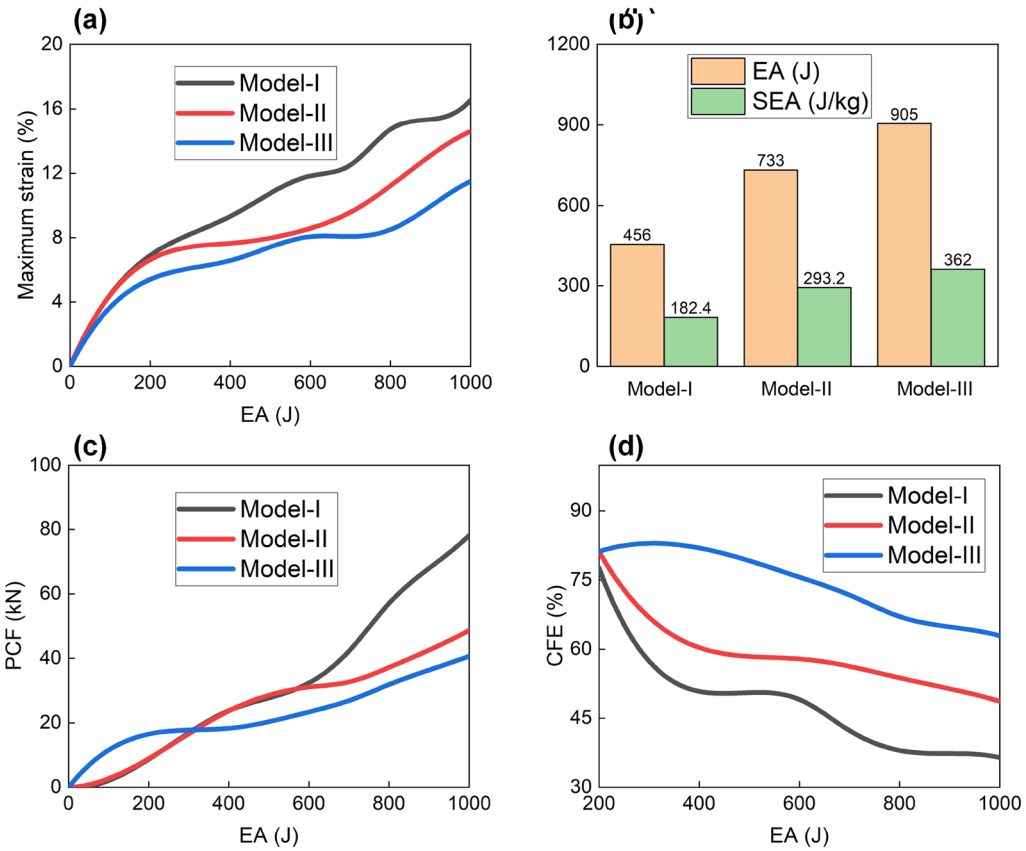

Figure 14 Energy absorption performance for three models with varied configurations: **a** Maximum strain curves, **b** Comparison of EA and SEA, **c** PCF curves, **d** CFE curves

approximately 10%, 5%, and 6%, respectively. The deformation of the Model-I is not as uniform as the other two models.

As shown in Figure 14, the simulation results show that the maximum strain and PCF for all three configurations increase with absorbed energy, while CFE decreases with energy. Comparison between configurations 1 and 2 reveals that the latter has a lower maximum strain value under similar impact conditions, resulting in improved energy absorption performance. At an absorbed energy of approximately 700 J, Model-II exhibits a lower impact deformation compared to Model-I, with CFE exceeding 20% of Model-I thereby demonstrating superior energy absorption performance. Meanwhile, it is noteworthy

that the shear deformation phenomenon of cells will weaken the energy-absorption capacity of a certain structure, which is also presents a positive correlation to the uniform deformation mode.

The simulation results indicate that Model-III exhibits better performance in terms of the maximum strain, CFE, PCF, and EA compared to Configurations 1 and 2 when subjected to equal impact energy. By analyzing the slope of the PCF curve, it indicates that the initial compression stiffness of Model-III is approximately 50% more than that of the other two configurations, causing it to reach the plateau stress earlier and making the PCF curve smoother. This reduction of shear deformation in the outer cells enhances the compressive stiffness of the footpad in the vertical direction and is beneficial to improve the energy absorption of the two-stage energy absorption structure with variable stiffness. In this study, Model-III is selected as an optimal structure due to its superior performance under the defined impact conditions.

4.2 Influence of Thickness Parameters

When the configuration of the footpad is fixed, the wall thickness is an important factor in determining the compression stiffness of the structure. The effect of thickness on energy absorption performance was studied when multi-cell metal thin-walled structures were subjected to transverse compression in Ref. [46], and the results demonstrate that the uneven distribution of thickness in the configuration has a significant impact on the overall deformation mode. As previously discussed, the stiffness of the inner and outer structures plays a significant role in the energy absorption capacity of the two-stage configuration footpad with variable stiffness. According to the deformation mode of the footpad, the honeycomb structure filled with the configuration is divided into inner and outer structures, the thickness of which is expressed by the following equation:

$$\begin{cases} t_{ineer} = 0.71 + n, \\ t_{outer} = 0.71 - \frac{S_{inner}}{S_{outer}} \times n, \end{cases} r = \frac{t_{ineer}}{t_{outer}} \in [0.6,\ 1.6], \tag{8}$$

where t_{ineer} and t_{outer} represent the thickness of the inner and outer thin-walled structure, respectively; S_{inner} and S_{outer} are the areas of the inner and outer structures, r is the thickness ratio of the inner and outer structure; n is the thickness adjustment parameter. We investigate the impact of varying the thickness of the inner and outer structures, and optimizes the design accordingly. The finite element analysis is performed using Model-III with the same boundary conditions, and the thickness ratio between the inner and outer structures is varied within the range [0.6, 1.6] to maintain the constant total mass of the footpad structure at 2.5 kg.

The energy performance of the designed footpad structures, considering the varying thickness factors, has been determined by means of numerical simulations. As shown in Figure 15, the absorbed energy of the footpad exhibits a positive correlation with the thickness of the inner structure and a negative correlation with the thickness of the outer structure. The CFE initially increases and then decreases as the ratio of inner to outer structure thickness increases. The maximum CFE value is found to be greater than 52% when the thickness ratio is approximately 0.86, representing a 2.34% improvement over the original design.

The impact energy of the lander is primarily governed by the total mass of the payload system. The energy absorption capabilities of the footpad, in terms of its SFE, are not fully utilized under low impact loads, whereas excessive impact loads may lead to local damage or failure in the footpad. To address this issue, the impact of varying thickness on the energy absorption performance of the footpad is analyzed in this study. The findings can provide a theoretical basis for the design of reusable footpads or comprehensive landing energy absorption systems.

5 Conclusions

(1) In this study, a design methodology for energy absorption structures using shape memory alloy (SMA) material is proposed. Specifically, the maximum recoverable strain is introduced as a design constraint. A reusable footpad for a lander is designed through a two-stage design approach. An ESL-based topology optimization is conducted to obtain a general configuration, which serves as the basis for a detailed prototype design. Subsequently, honeycomb-like cellular structures are employed to replace the original configuration.

(2) The numerical simulations of the honeycomb-like local structure, which is representative of the overall structure, demonstrate a good agreement with the experimental results. This finding not only validates the modeling approach proposed in this study but also highlights its accuracy. Furthermore, irrespective of the recovery process of SMA material, the linear piecewise material model can be effectively employed to examine the energy absorption performance of SMA fabricated structures subjected to impact loads.

(3) Finite element method is employed to conduct a quantitative analysis of the influence of different configurations and design parameters on the energy absorption performance of the lander footpad. The findings indicate that shear band can significantly diminish the energy absorption capacity of honeycomb-like structures, highlighting the need to consider this factor in the design of reusable SMA structures. Under the

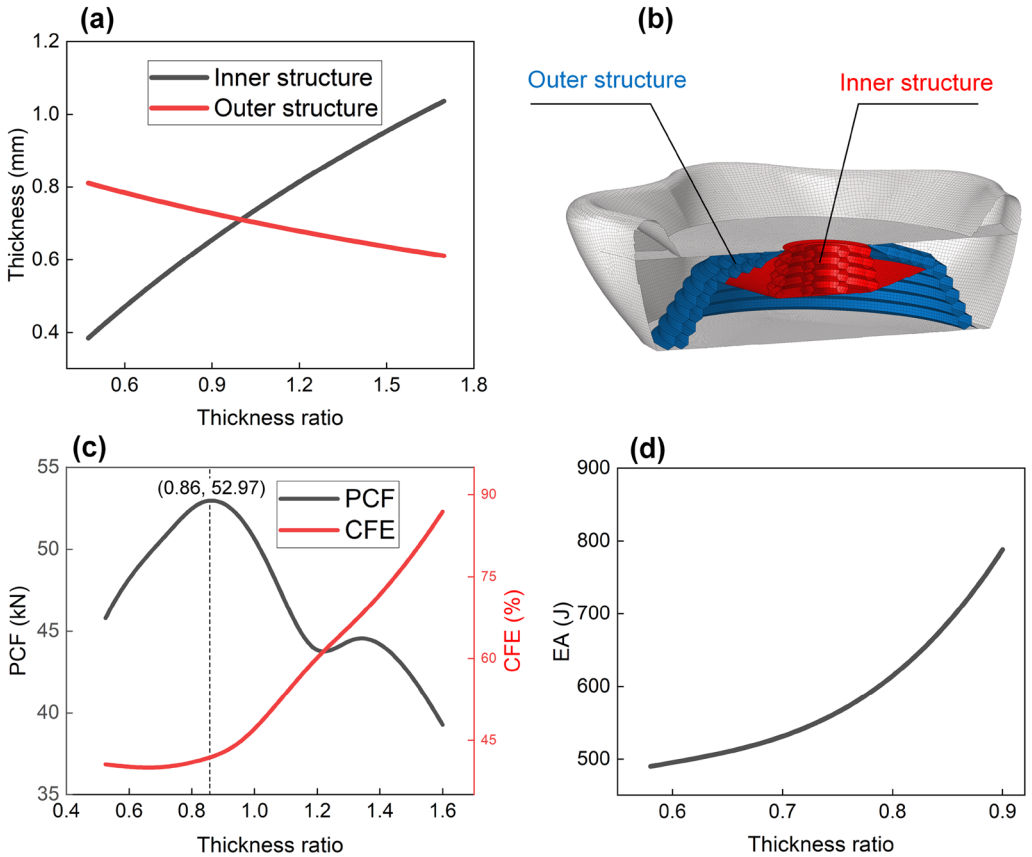

Figure 15 Influence of inner and outer structure thickness ratio: **a** Thickness change between inner structure and outer structure, **b** The finite element model showing the inner and outer structures, **c** PCF and CFE curves with respect to thickness ratio, **d** EA curve with respect to thickness ratio

constraint of the maximum recoverable strain of SMA, the designed reusable footpad structure achieves an energy absorption capacity of 362 J/kg, with a crushing force efficiency greater than 63%. In future studies, a reusable landing gear will be investigated to compose an integrated system with the proposed footpad, and more experiments will be necessary to validate its practicability further.

Acknowledgements
The authors sincerely thanks to Professor Shijie Hao of China University of Petroleum for his full support in this study.

Authors' Contributions
WD wrote the manuscript and was in charge of the whole trial; XQ and YG assisted geometric modeling and numerical simulation; ZX conducted the experiment; LZ assisted review and editing. All authors read and approved the final manuscript.

Authors' Information
Weiyuan Dou born in 1989, is currently a lecturer at *School of Mechanical, Electronic, and Control Engineering, Beijing Jiaotong University, China*. His research interests include multi-field coupling, structural design and optimization, and numerical simulation methods.
Xiaohang Qiu born in 2001, is currently an undergraduate student at *School of Mechanical, Electronic and Control Engineering, Beijing Jiaotong University, China.*
Zhiwei Xiong born in 1993, is currently an engineer at China Academy of Space Technology.
Yanzhao Guo born in 2000, is currently a PhD candidate at *School of Mechanical, Electronic and Control Engineering, Beijing Jiaotong University, China.*
Lele Zhang born in 1973, is currently a professor at *School of Mechanical, Electronic, and Control Engineering, Beijing Jiaotong University, China*. Her research interests include passive safety and optimization design.

Funding
Supported by Fundamental Research Funds for the Central Universities of China (Grant No. 2021JBM021), and National Natural Science Foundation of China (Grant Nos. 52202431, 52172353).

Data Availability
Data will be made available on request.

Declarations

Competing Interests
The authors declare no competing financial interests.

Received: 20 February 2023 Revised: 17 July 2023 Accepted: 20 July 2023
Published online: 22 August 2023

References

[[1] D C Arney, C A Jones, J Klovstad, et al. Sustaining human presence on mars using ISRU and a reusable lander. *AIAA Space 2015 Conference and Exposition*, 2015: 4479.

[2] B Robertson, E M Ramos, M J Diaz, et al. A conceptual design study for an unmanned, reusable cargo lunar lander. *International Astronautical Congress (IAC)*, 2019: IAC-19-D2.4.10.

[3] D Carabellese, D Barbero, P Pino, et al. Preliminary design of a reusable lunar lander/ascender for on-orbit refueling. *AIAA Propulsion and Energy 2020 Forum*, 2020: 3531.

[4] B Huang, Z Jiang, P Lin, et al. Research on impact process of lander footpad against simulant lunar soils. *Shock and Vibration*, 2015: 658386.

[5] C Wang, H Nie, J Chen, et al. The design and dynamic analysis of a lunar lander with semi-active control. *Acta Astronautica*, 2019, 157: 145-156.

[6] X Xu, Y Zhang, X Wang, et al. Searching superior crashworthiness performance by constructing variable thickness honeycombs with biomimetic cells. *International Journal of Mechanical Sciences*, 2022, 235: 107718.

[7] Y Zhang, X Xu, J Fang, et al. Load characteristics of triangular honeycomb structures with self-similar hierarchical features. *Engineering Structures*, 2022, 257: 114114.

[8] H Li, Y Liu, H Zhang, et al. Amplitude-dependent damping characteristics of all-composite sandwich plates with a foam-filled hexagon honeycomb core. *Mechanical Systems and Signal Processing*, 2023, 186: 109845.

[9] Y Liu, X Shi, Z Wang, et al. Nonlinear vibrations of all-composite sandwich plates with a hexagon honeycomb core: Theoretical and experimental investigations. *Composite Structures*, 2023, 305: 116512.

[10] V V Selivanov, M V Silnikov, V A Markov, et al. Using highly porous aluminum alloys and honeycomb structures in spacecraft landing gear. *Acta Astronautica*, 2021, 180: 105-109.

[11] W Wei, S Zhang, X Zhao, et al. Research on aluminum honeycomb buffer device for soft landing on the lunar surface. *International Journal of Aerospace Engineering*, 2021: 1-20.

[12] M Li, Z Deng, R Liu, et al. Crashworthiness design optimisation of metal honeycomb energy absorber used in lunar lander. *International Journal of Crashworthiness*, 2011, 16(4): 411-419.

[13] B Lei, M Zhang, H Lin, et al. Optimization design containing dimension and buffer parameters of landing legs for reusable landing vehicle. *Chinese Journal of Aeronautics*, 2022, 35(3): 234-249.

[14] Z Ding, H Wu, C Wang, et al. Hierarchical optimization of landing performance for lander with adaptive landing gear. *Chinese Journal of Mechanical Engineering*, 2019, 32: 1-12.

[15] H Yu, B Tian, Z Yan, et al. Watt linkage–based legged deployable landing mechanism for reusable launch vehicle: Principle, prototype design, and experimental validation. *Engineering*, 2023, 20: 120-133.

[16] G Song, N Ma, H Li. Applications of shape memory alloys in civil structures. *Engineering Structures*, 2006, 28(9): 1266-1274.

[17] M L Lapér, R Guimaraes, B R Barrioni, et al. Fabrication of porous samples from a high-temperature Cu–Al–Ni–Mn–Nb shape memory alloy by freeze-drying and partial sintering. *Journal of Materials Research and Technology*, 2020, 9(3): 3676-3685.

[18] O Ammar, N Haddar, L Dieng. Experimental investigation of the pseudoelastic behaviour of NiTi wires under strain-and stress-controlled cyclic tensile loadings. *Intermetallics*, 2017, 81: 52-61.

[19] L Marandi, I Sen. In-vitro mechanical behavior and high cycle fatigue characteristics of NiTi-based shape memory alloy wire. *International Journal of Fatigue*, 2021, 148: 106226.

[20] J P Oliveira, Z Zeng, S Berveiller, et al. Laser welding of Cu-Al-Be shape memory alloys: Microstructure and mechanical properties. *Materials & Design*, 2018, 148: 145-152.

[21] C Qiu, S Zhu. Characterization of cyclic properties of superelastic monocrystalline Cu–Al–Be SMA wires for seismic applications. *Construction and Building Materials*, 2014, 72: 219-230.

[22] Y Tanaka, Y Himuro, R Kainuma, et al. Ferrous polycrystalline shape-memory alloy showing huge superelasticity. *Science*, 2010, 327(5972): 1488-1490.

[23] G Crowther, D D Apostolopoulos, S Heys. Tensegrital wheel for enhanced planetary surface mobility: Part 1–Design and evolution. *Journal of Terramechanics*, 2022, 100: 11-24.

[24] H Lu, L Liu, C Yang, et al. Simultaneous enhancement of mechanical and shape memory properties by heat-treatment homogenization of Ti2Ni precipitates in TiNi shape memory alloy fabricated by selective laser melting. *Journal of Materials Science & Technology*, 2022, 101: 205-216.

[25] O Benafan, J Brown, F T Calkins, et al. Shape memory alloy actuator design: CASMART collaborative best practices and case studies. *International Journal of Mechanics and Materials in Design*, 2014, 10: 1-42.

[26] Z Xiong, Z Li, Z Sun, et al. Selective laser melting of NiTi alloy with superior tensile property and shape memory effect. *Journal of Materials Science & Technology*, 2019, 35(10): 2238-2242.

[27] Z Xiong, H Li, H Yang, et al. Micro laser powder bed fusion of NiTi alloys with superior mechanical property and shape recovery function. *Additive Manufacturing*, 2022, 57: 102960.

[28] Z Xiong, M Li, S Hao, et al. 3D-printing damage-tolerant architected metallic materials with shape recoverability via special deformation design of constituent material. *ACS Applied Materials & Interfaces*, 2021, 13(33): 39915-39924.

[29] B S Kang, W S Choi, G J Park. Structural optimization under equivalent static loads transformed from dynamic loads based on displacement. *Computers & Structures*, 2001, 79(2): 145-154.

[30] G J Park, B S Kang. Validation of a structural optimization algorithm transforming dynamic loads into equivalent static loads. *Journal of Optimization Theory and Applications*, 2003, 118: 191-200.

[31] C H Chuang, S Chen, R J Yang, et al. Topology optimization with additive manufacturing consideration for vehicle load path development. *International Journal for Numerical Methods in Engineering*, 2018, 113(8): 1434-1445.

[32] N M Patel, B S Kang, J E Renaud, et al. Crashworthiness design using topology optimization. *Journal of Mechanical Design*, 2009, 131(6): 061013.

[33] N Aulig, E Nutwell, S Menzel, et al. Preference-based topology optimization for vehicle concept design with concurrent static and crash load cases. *Structural and Multidisciplinary Optimization*, 2018, 57: 251-266.

[34] A A Nia, M Parsapour. Comparative analysis of energy absorption capacity of simple and multi-cell thin-walled tubes with triangular, square, hexagonal and octagonal sections. *Thin-Walled Structures*, 2014, 74: 155-165.

[35] Q He, Y Wang, H Gu, et al. The dynamic behavior of fractal-like tubes with Sierpinski hierarchy under axial loading. *Engineering with Computers*, 2022: 1-14.

[36] H S Abdullahi, S Gao. A novel multi-cell square tubal structure based on Voronoi tessellation for enhanced crashworthiness. *Thin-Walled Structures*, 2020, 150: 106690.

[37] S Wang, H Wang, Y Ding, et al. Crushing behavior and deformation mechanism of randomly honeycomb cylindrical shell structure. *Thin-walled structures*, 2020, 151: 106739.

[38] D Zhang, Q Fei, J Liu, et al. Crushing of vertex-based hierarchical honeycombs with triangular substructures. *Thin-Walled Structures*, 2020, 146: 106436.

[39] C Cisse, W Zaki, T B Zineb. A review of constitutive models and modeling techniques for shape memory alloys. *International Journal of Plasticity*, 2016, 76: 244-284.

[40] P Motamarri, A Ramani, A Kaushik. Structural topology synthesis with dynamics and nonlinearities using equivalent linear systems. *Structural and Multidisciplinary Optimization*, 2012, 45(4): 545-558.

[41] X Wei, Q Lin, H Nie, et al. Investigation on soft-landing dynamics of four-legged lunar lander. *Acta Astronautica*, 2014, 101: 55-66.

[42] Y B Kim, H J Jeong, S M Park, et al. Prediction and validation of landing stability of a lunar lander by a classification map based on touchdown landing dynamics' simulation considering soft ground. *Aerospace*, 2021, 8(12): 380.

[43] C Yin, P Schiavone, Q Quan, et al. Normal force on the asteroid regolith generated by the impact of lander footpad. *Acta Astronautica*, 2023, 202: 229-251.

[44] Y Wu, L Sun, P Yang, et al. Energy absorption of additively manufactured functionally bi-graded thickness honeycombs subjected to axial loads. *Thin-Walled Structures*, 2021, 164: 107810.

[45] M O Ayanoglu, M Tauhiduzzaman, L A Carlsson. In-plane compression modulus and strength of Nomex honeycomb cores. *Journal of Sandwich Structures & Materials*, 2022, 24(1): 627-642.

[46] M Kazemi, J Serpoush. Energy absorption parameters of multi-cell thin-walled structure with various thicknesses under lateral loading. *Proceedings of the Institution of Mechanical Engineers, Part L: Journal of Materials: Design and Applications*, 2021, 235(3): 513-526.